Original Paper

Caries Research

Caries Res 2004;38:497–513
DOI: 10.1159/000080579

Received: August 1, 2003
Accepted after revision: February 24, 2004

Diagnosis of Pit and Fissure Caries Using Frequency-Domain Infrared Photothermal Radiometry and Modulated Laser Luminescence

R.J. Jeon[a] C. Han[a] A. Mandelis[a] V. Sanchez[a] S.H. Abrams[b]

[a] Center for Advanced Diffusion-Wave Technologies, Department of Mechanical and Industrial Engineering, University of Toronto, and [b] Four Cell Consulting, Toronto, Ont., Canada

Key Words

Dental caries diagnosis · Dental photothermal radiometry · Frequency scans · Modulated luminescence · Pit and fissure caries

Abstract

Non-intrusive, non-contacting frequency-domain photothermal radiometry (FD-PTR or PTR) and frequency-domain luminescence (FD-LUM or LUM) have been used with 659- and 830-nm laser sources to assess the pits and fissures on the occlusal surfaces of human teeth. Fifty-two human teeth were examined with simultaneous measurements of PTR and LUM and were compared to conventional diagnostic methods including continuous (dc) luminescence (DIAGNOdent), visual inspection and radiographs. To compare each method to the others, sensitivities and specificities were calculated by using histological observations as the gold standard. With the combined criteria of four PTR and LUM signals (two amplitudes and two phases), it was found that the sensitivity of this method was much higher than any of the other methods used in this study, whereas the specificity was comparable to that of dc luminescence diagnostics. Therefore, PTR and LUM, as a combined technique, has the potential to be a reliable tool to diagnose early pit and fissure caries and could provide detailed information about deep lesions. Using the longer wavelength (830-nm) laser source, it has been shown that detection of deeper subsurface lesions than the 659-nm probe provides is possible.

Over the last few decades with the widespread use of fluoride, the prevalence of caries, particularly smooth surface caries, has been considerably reduced [Ricketts et al., 1997; McComb and Tam, 2001]. This reduction in smooth surface caries has resulted in an increase in the proportion of small lesions in the pits and fissures of teeth [McComb and Tam, 2001]. The diagnosis of pit and fissure caries continues to be a dilemma for clinicians. Caries detection for the vast majority of clinicians still relies upon radiographs, explorer and visual determination. With these 'crude' tools, clinicians are hampered in their ability to diagnose and monitor the carious lesion or assess the status of a stained pit or fissure. There are no clear guidelines on their clinical management and one clinical research group has suggested that carious defects are almost always present under stained pits and fissures of

KARGER

Fax +41 61 306 12 34
E-Mail karger@karger.ch
www.karger.com

0008–6568/04/0386–0497$21.00/0

Accessible online at:
www.karger.com/cre

Prof. A. Mandelis
Center for Advanced Diffusion-Wave Technologies
Department of Mechanical and Industrial Engineering, University of Toronto
5 King's College Road, Toronto, Ont. M5S 3G8 (Canada)
Tel. +1 416 978 5106, Fax +1 416 978 5106, E-Mail mandelis@mie.utoronto.ca

non-smokers [Clinical Research Associates, 1999]. The development of a non-invasive, non-contacting technique or instrument which can detect early demineralization on or beneath the enamel surface is essential for the clinical management of this problem.

The use of lasers for dental diagnostics is considered to be promising, mainly through the phenomenon of laser-induced fluorescence (or luminescence) of the enamel. Eggertsson et al. [1999] evaluated the uses of laser fluorescence and dye-enhanced laser fluorescence (DELF), compared them to visual examination and found DELF was better in sensitivity, but DELF and visual examination were better than laser fluorescence in specificity. In an effort to quantify the fluorescence-based light-induced fluorescence technique, various devices such as a ring illuminator, a beam splitter and a clinical caries camera were compared by Lagerweij et al. [1999]. The DIAGNOdent [Hibst and Konig, 1994; Hibst et al., 2000] uses laser excitation at 655 nm to distinguish between carious and healthy tooth structure. The measured quantity is steady-state (equilibrium) luminescence (the authors equivalently use the term 'fluorescence'), albeit the laser beam is chopped at a fixed frequency to minimize background light interference. Nevertheless, the DIAGNOdent does not explore the physical relaxation mechanisms of the non-steady (dynamic) character of modulated luminescence [Nicolaides et al., 2000] as a diagnostic means of tooth integrity. For this reason, in our work we refer to it as a 'dc luminescence measuring device', meaning a physical quantity at thermodynamic equilibrium. The device is based upon the fluorescence caused by porphyrins present in carious tissue and not the amount of enamel demineralization [Alwas-Danowska et al., 2002]. Porphyrin fluorescence may lead to false positives since porphyrins are also found in stained, healthy fissures [Hibst and Paulus, 1999; Welsh et al., 2000]. A number of studies were performed to assess the feasibility of using this device [Lussi et al., 1999; Shi et al., 2000, 2001], and it has been evaluated as having the potential to improve caries assessment in many ways. Specifically, its high reproducibility was claimed to be an outstanding benefit of this device. Nevertheless, a validity study involving the DIAGNOdent concluded that using dc luminescence was not statistically significantly different from visual inspection [Alwas-Danowska et al., 2002]. Furthermore, it was concluded that the DIAGNOdent was suitable for detecting small superficial lesions, rather than deep dentinal lesions [Alwas-Danowska et al., 2002]. There are various sensitivity and specificity values obtained for the DIAGNOdent and they differ widely among different researchers, 0.76–1.00 for the sensitivity and 0.47–0.94 for the specificity [Lussi et al., 1999, 2001; Alwas-Danowska et al., 2002; Costa et al., 2002; Heinrich-Weltzien et al., 2002; Anttonen et al., 2003].

The first attempt to apply the depth profilometric capability of frequency-domain laser infrared photothermal radiometry (PTR) toward the inspection of dental defects was reported by Mandelis et al. [2000] and Nicolaides et al. [2000] and was recently reviewed by Mandelis [2002]. The approach consists of a combined dynamic (i.e. non-static, steady-state signal level) dental depth profilometric inspection technique, which can provide simultaneous measurements of intensity-modulated frequency-domain PTR (FD-PTR) and luminescence (FD-LUM) signals from defects in teeth. FD-PTR is an evolving technology and has been applied, among other areas, to the non-destructive evaluation of subsurface features in opaque materials [Busse and Walther, 1992]. It has shown promise in the study of excited-state dynamics in optically active solid-state (laser) materials [Mandelis et al., 1993]. The technique is based on the modulated thermal infrared (black-body or Planck radiation) response of a medium, resulting from radiation absorption and non-radiative energy conversion followed by temperature rise (in the case of dental interrogation, less than 1 °C). The generated signals carry subsurface information in the form of a temperature depth integral. Thus, PTR has the ability to penetrate, and yield information about, an opaque medium well beyond the range of optical imaging. Specifically, the frequency dependence of the penetration depth of thermal waves makes it possible to perform depth profiling of materials [Munidasa and Mandelis, 1992]. In PTR applications to turbid media, such as hard dental tissue, depth information is obtained following optical-to-thermal energy conversion and transport of the incident laser power in two distinct modes: conductively, from a near-surface distance controlled by the thermal diffusivity of enamel (50–500 μm) [Brown et al., 1970]; and radiatively, through blackbody emissions from considerably deeper regions commensurate with the optical penetration of the diffusely scattered laser-induced optical field (several millimetres) [Nicolaides et al., 2002].

It is often desirable in dental practice to obtain detailed information on potential lesions or to examine pits and fissures with high spatial resolution, using a focused laser source. To meet these objectives, recently, a combination of FD-PTR and FD-LUM was used as a fast dental diagnostic tool to quantify sound enamel or dentin as well as subsurface cracks in human teeth [Nicolaides et

al., 2000]. Under 488-nm laser excitation and frequencies in the range of 10 Hz to 10 kHz, it was found that PTR images are complementary to LUM images as a direct result of the complementary nature of non-radiative and radiative de-excitation processes, which are responsible for the PTR and LUM signal generation, respectively, at that wavelength. It was also concluded qualitatively that radiometric images are depth profilometric (meaning they yield depth-dependent information as a function of the laser-beam modulation frequency), but no definitive conclusions regarding the depth profilometric character of LUM were reached. Finally, LUM frequency responses from enamel and hydroxyapatite were found to exhibit two relaxation lifetimes, the longer of which (ms) is a benchmark hydroxyapatite relaxation lifetime common to all teeth and is not sensitive to the defect state or the overall quality of the enamel. A degree of sensitivity to enamel quality was established for the shorter (μs) lifetime. Our group has introduced theoretical models of FD-PTR and FD-LUM which can yield quantitative values of optical and fluorophore parameters of sound enamel [Nicolaides et al., 2002]. Unique sets of the optical parameters ($\overline{\mu}_a$: optical absorption coefficient, μ_s: scattering coefficient, μ_{IR}: spectrally averaged infrared emission coefficient) of enamel and its fluorophore relaxation time constants (τ_1, τ_2) were obtained using the combined diffuse photon-density-wave and thermal-wave theory with a three-dimensional photothermal multiparameter fit formulation and inputs from LUM and PTR data [Nicolaides et al., 2002]. More recently, it was found that PTR (alone or in combination with LUM) could be used as a sensitive, depth-profilometric dental probe for the diagnosis of near-surface or deep subsurface carious lesions and/or for monitoring enamel thickness [Jeon et al., 2004].

In this study, human teeth were examined to evaluate the diagnostic capabilities of FD-PTR and FD-LUM and compared to DIAGNOdent as well as visual inspection and radiographs. After the measurements were completed, the teeth were sectioned. Histological findings were used as the gold standard to calculate and compare the sensitivity and the specificity of all the diagnostic methodologies used in this study. Furthermore, to study the difference of optical penetration depth according to the wavelength of the source, frequency scans with two laser probes (659 nm and 830 nm) were performed and compared.

Materials and Methods

Fifty-two extracted human teeth (25 molars, 21 bicuspids and 6 primary molars) were evaluated. The measured points included, at a minimum, two healthy areas and two fissures on the occlusal surface and one healthy point on the smooth side surface. A few more measured points were added for each tooth, so the total measurement sample finally consisted of 332 points, including 104 healthy points, 176 fissures on the occlusal surface, and 52 healthy points on the smooth surfaces of the teeth. In order to compare our experimental results to other clinical methods, 5 dentists examined and ranked the set of teeth by visual inspection and radiographs. DIAGNOdent (KAVO model 2095) measurements were also obtained from the occlusal surfaces of the teeth. The visual inspection, radiograph and DIAGNOdent examination were performed earlier than the PTR and LUM experiment, and more points to measure for the PTR and LUM were added later. Therefore the numbers of the sample points for each examination method are different.

Tooth samples were stored in 0.9% sodium chloride separately in vials before the experiments to avoid dehydration and contamination. The occlusal surface of each tooth was photographed with a CCD camera (PULNiX TMC-73M) equipped with a magnification lens (NAVITAR Zoom6000) and the measurement points were selected and marked on each photograph.

Visual Inspection and Radiography

Five clinicians were given sample teeth, which had been stored in saline solution, and asked to assess them with respect to clinical criteria. They were asked to assess only the occlusal surface of each tooth, specifically the pits and fissures. The clinicians were not asked to state whether the caries was in enamel or dentin but whether they would treat the tooth and in what manner. This is very similar to what a dentist does clinically on a day-to-day basis with treatment recommendations ranging from no treatment, to watching a suspect fissure, placement of a sealant to the placement of a large or small restoration. We provided each clinician with a tooth, explorer, oil-free air, and a radiograph of the tooth. The clinicians were asked to assign a ranking from 1 to 10 for each tooth with 1 meaning no treatment was required and 10 meaning that a large carious lesion was present involving the dentin and enamel (table 1). The clinicians were not asked to assess each fissure, only to rank the status of all fissures on the occlusal surface of a particular tooth. Rankings were further divided into four groups with the classification scheme described in table 1.

Radiographic Examination

A radiograph was taken on each tooth using standard dental X-rays. The teeth were each mounted on a jig that fixed the distance between film, tooth and X-ray tube head. This ensured similar magnification and exposure. Each radiograph was examined by all clinicians independently of the visual exam to detect the presence of occlusal caries. The teeth were mounted with no adjacent teeth since we were only interested in examining the occlusal and not interproximal surfaces.

DIAGNOdent

Each tooth was dried and the DIAGNOdent instrument was used to obtain readings from the occlusal surface. The machine was calibrated between each tooth and the surface was scanned 3 times

Table 1. Diagnostic criteria for the visual inspection, DIAGNOdent, X-ray and histological observation

General description of levels of caries [Lussi et al., 1999]	Visual inspection (1–10)	DIAGNOdent (0–99) [Lussi et al., 1999]	Radiography	Histological observation
D_0: intact			healthy: indicating no sign of demineralization	sound enamel or healthy fissure
D_1: no caries, or histological enamel caries limited to the outer half of the enamel thickness	1–2 incipient or healthy fissures, observe and monitor	0–4	enamel caries under 1/2 the distance to DEJ	demineralized fissure but solid enamel base; very good enamel thickness to the pulp; at least 1/2 thickness of enamel remains intact
D_2: histological caries extending beyond the outer half, but confined to the enamel	3–5 fissures are suspicious but not carious, fissure sealant recommended as treatment	4.01–10	enamel caries greater than 1/2 the distance to DEJ	demineralized fissure but solid enamel base
D_3: histological dentinal caries limited to the outer half of the dentin thickness	6–8 caries needing the placement of a restoration, restore the fissure	10.01–18	dentin caries	caries into dentin
D_4: histological dentinal caries extending into the inner half of dentin thickness	9–10 large carious lesion, caries deep into dentin	>18.01		

DEJ = Dentin-enamel junction.

to confirm the reading. The highest reading on the occlusal surface and its location were recorded. The readings were assessed and ranked using the criteria developed by Lussi et al. [1999] and listed in table 1.

Sample Preparation before PTR and LUM Scanning

Each sample tooth in the study was removed from the vial and was rinsed thoroughly with clean water for more than 20 s and then was dried with pressurized air. Then, the tooth was placed on the sample stage, and the laser was turned on and focused on the sample tooth by adjusting a three-axis micrometer stage. This process usually took about 20 min before starting measurements, during which time the tooth was dehydrated properly. This protocol was adhered to, because dehydration of a tooth sample affects its optical qualities, such as light scattering and fluorescence as well as thermal properties. Al-Khateeb et al. [2002] showed that the fluorescence radiance of sound enamel and enamel lesions decreased from that of the wet enamel for about 2–20 min, depending on the sample, before becoming steady. Therefore, 20 min of preparation time appears to be necessary to avoid the effects of dehydration or the signals. Moreover, since the surface temperature of the sample could be slightly decreased during washing with water and drying with compressed air, there was a need to wait until the sample temperature reached its ambient value, because modulated luminescence and thermal infrared (blackbody) emissions may be affected by the background temperature.

PTR and LUM Measurements

Figure 1 shows the experimental setup for combined frequency-domain PTR and LUM probing. Two semiconductor lasers with wavelength 659 nm (maximum power 30 mW; Mitsubishi ML1016R-01) and with 830 nm (maximum power 100 mW, Sanyo DL-7032–001) were used as the sources of both PTR and LUM signals. A diode laser driver (Coherent 6060) was used for the laser and was triggered by the built-in function generator of the lock-in amplifier (Stanford Research SR830), modulating the laser current harmonically. The laser beam was focused on the sample with high performance lenses (Gradium GPX085, focal length: 200 mm) to a spot size of 53.3 ± 2.0 μm for the 659-nm laser and 325.9 ± 25.5 μm for the 830-nm laser, which were measured with a 3-μm diameter pinhole. The modulated infrared PTR signal from the tooth was collected and focused by two off-axis paraboloidal mirrors (Melles Griot 02POA019, rhodium-coated) onto a mercury cadmium telluride (HgCdTe or MCT) detector (EG&G Judson J15D12-M204-S050U). Before being sent to the lock-in amplifier, the PTR signal was amplified by a preamplifier (EG&G Judson PA-300). For the simultaneous measurement of PTR and LUM signals, a germanium window was placed between the paraboloidal mirrors

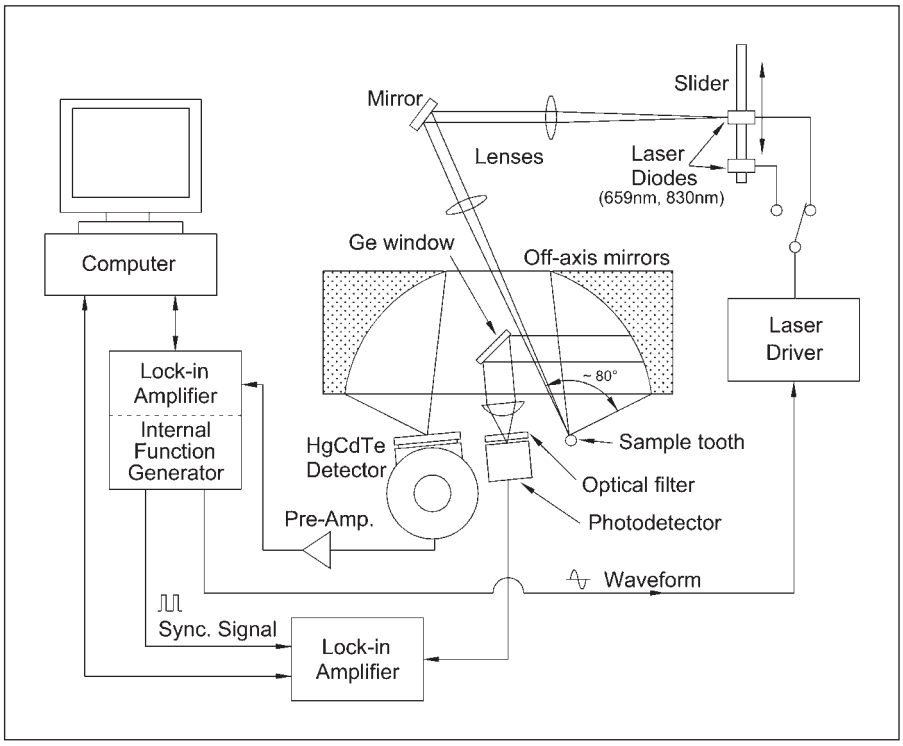

Fig. 1. Schematic diagram of experimental setup.

so that wavelengths up to 1.85 μm (Ge bandgap) would be reflected and absorbed, while infrared radiation with longer wavelengths would be transmitted. The reflected luminescence was focused onto a photodetector of spectral bandwidth 300 nm to 1.1 μm (Newport 818-BB-20). A cut-on coloured glass filter (Oriel 51345, cut-on wavelength: 715 nm) was placed in front of the photodetector for luminescence to block laser light reflected or scattered by the tooth. No luminescence data were possible under 830 nm excitation, since photoluminescence emission requires irradiation with higher photons than the peaks of luminescence at approximately 636, 673 and 700 nm [Hibst and Konig, 1994]. We tested 695- and 725-nm filters as well as a715-nm filter and found the 715-nm filter was optimal for cutting off the laser source (659 nm) and cutting on the luminescence with negligible leakage signal (about 190 times less than the minimum dental LUM signals we obtained). Therefore, the 715-nm cut-on filter was used to measure the luminescence for only the 659-nm laser. For monitoring the modulated luminescence, another lock-in amplifier (EG&G model 5210) was used. Both lock-in amplifiers were connected to, and controlled by, the computer via RS-232 ports.

This experimental setup resulted in a wide angle (~80°) between laser beam and infrared detector, collecting infrared radiation emitted from the tooth surface. This restriction created problems detecting signals from fissures with a narrow entrance angle, or fissures that tracked under a cuspal incline (especially mandibular premolars) or headed off on an extreme angle with respect to the occlusal surface. At each measurement point, a frequency scan was performed measuring the PTR and the LUM signals by varying the frequency from 1 Hz to 1 kHz. The frequency range was segmented into 40 equal intervals on a logarithmic scale by a data acquisition computer program and the frequency was incremented to the next value after each measurement. There was a 15-second time delay between the measurements at each frequency to allow for thermalization of the tooth surface, which was necessary for stabilizing the signals. All signals were maximized by rotating the surface of the tooth exposed to laser light so that the incidence was nearly normal to the surface. Using the micro-positioning stage, which is composed of a three-axis translation stage and a rotation stage, the position of the sample can be controlled precisely with a resolution of better than 5 μm. Signal reproducibility by a single operator was verified on a selected subset of samples which were repeatedly scanned to confirm the readings. Reproducibilities ranged from 89 to 99%. Reproducibility was assumed to be valid for the remainder of samples, which were treated in the same type of experiments (line and frequency scans).

Histology Observation

After all the measurements were finished, the teeth in our sample were sectioned and photographed with the CCD camera directed perpendicular to the surface at each measurement point. The photographs of the sectioned teeth were examined and ranked according to the criteria listed in table 1.

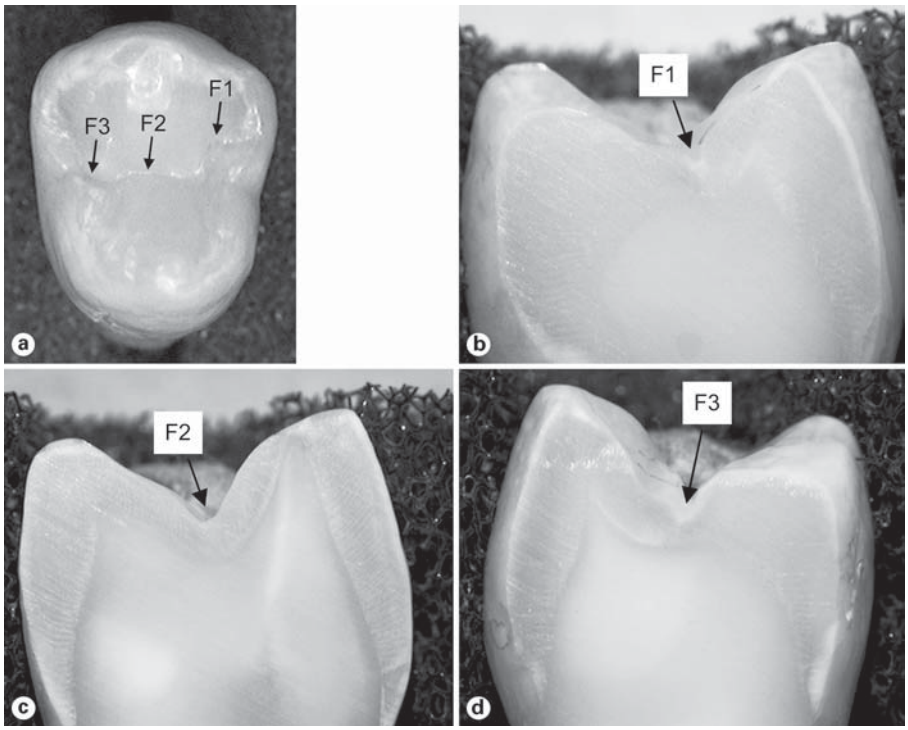

Fig. 2. A healthy tooth sample and its PTR and LUM signals using 659 nm excitation: occlusal view of the tooth (**a**); cross-sectioned view of each measurement point, F1, F2 and F3 (**b–d**); PTR (**e**, **f**) and LUM (**g**, **h**) amplitude and phase frequency scans at all the measurement points with the healthy mean value and population-weighted standard deviation.

Results and Discussion

PTR and LUM Measurements

Typical healthy and carious tooth samples and their PTR and LUM frequency responses are shown in figures 2 and 3, respectively. To identify each probed spot, the upper-case letter F (for fissure) and serial numbers were assigned. Also, the mean values, from all healthy smooth surface spots at each frequency, and their standard deviation bars, were added to each plot to compare the various curves.

Healthy Occlusal Fissures

Figure 2a shows the occlusal surface of a healthy tooth and its associated locations measured with the 659-nm laser source. This tooth had a DIAGNOdent reading of 4, average visual inspection ranking of 1.4 and no evidence of any caries on the radiographs. Thus there was no evidence of pathology in the fissures of this tooth. Histological observation shown in figure 2b–d also verified that all the measured points were healthy. In figure 2e, all PTR amplitude curves were located in between the healthy band or lower than its lower bound as determined by the standard deviation. Therefore, the diagnosis of these spots was 'healthy' as long as all other PTR and LUM signals did not show unhealthy behaviour, and exhibited a curve shape consistent with the healthy mean-value curve. PTR phase curves for fissures in figure 2f were slightly higher than the healthy mean and exhibited some curvature. This type of low curvature is very likely due to thermal-wave confinement in the fissure which represents a higher-dimension geometry [Mandelis, 2001, chapter 4] and is characteristic of healthy fissures; it lies essentially within the healthy PTR phase band and can be used as a diagnostic of healthy fissures. In general, a healthy tooth exhibited weaker PTR signals than carious teeth. This was the cause of poorer signal-to-noise ratios in both amplitude and phase curves. LUM amplitude curves for all probed points were below the healthy band in figure 2g and LUM phases were within the mean (fig. 2h). Note that LUM amplitudes and phases suffered from low signal-to-noise ratios in the high frequency range. In conclusion, all four signal channels for the spots in figure 2a supported a healthy assignment.

Carious Occlusal Fissures

The carious tooth in figure 3 had a DIAGNOdent reading of 12 in the mesial pit and a clinical ranking of 3.8. The radiograph did not indicate the presence of any carious lesion on the occlusal surface. There was a carious

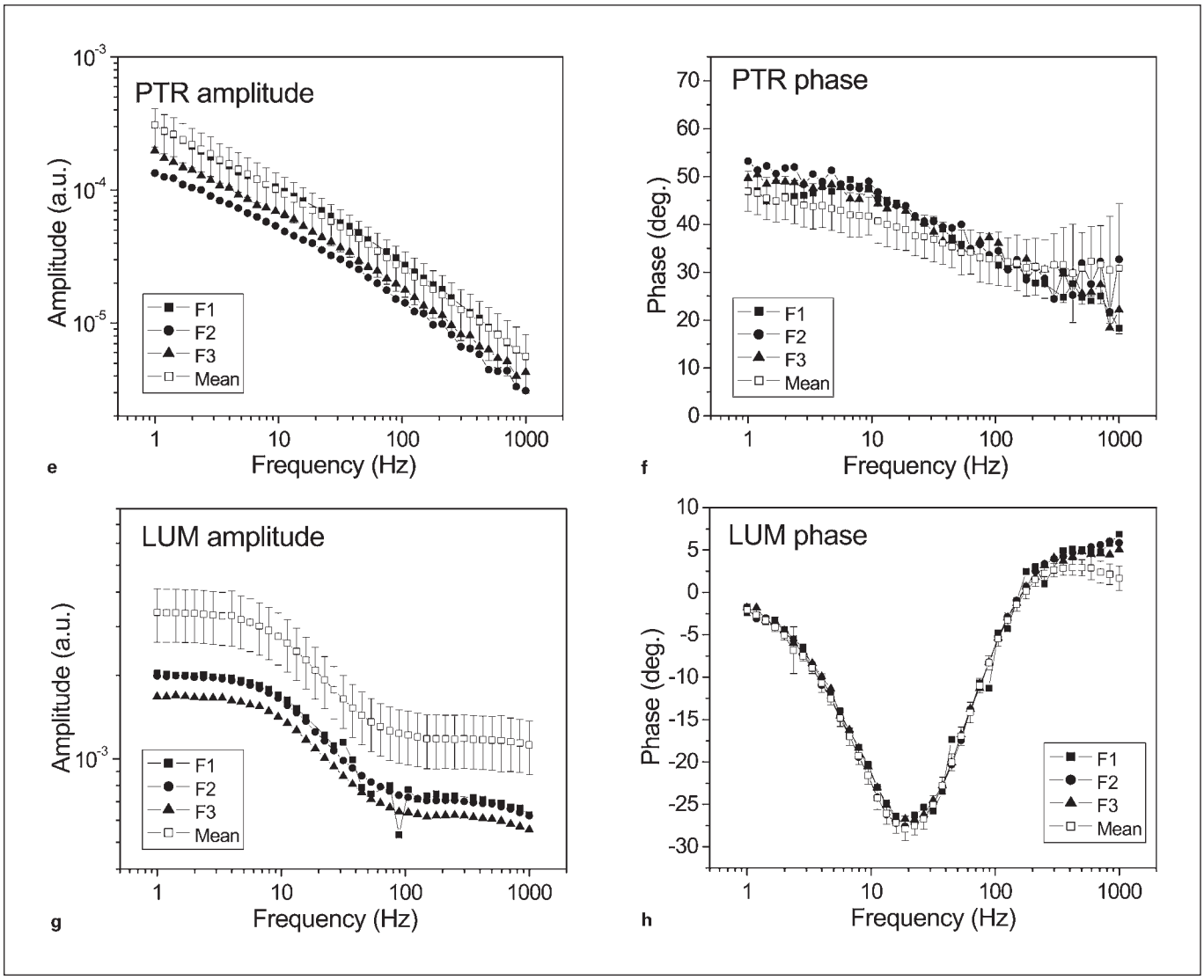

lesion on the distal surface of this tooth but only the occlusal surface was under examination. Histological observation found that the fissures F1 and F2 of this tooth were D_3 (histological dentinal caries limited to the outer half of the dentin layer) because of the demineralized lateral wall and base with black stain. These carious fissures exhibited clear differences from the healthy mean curves (fig. 3c–f), while the healthy points of the same tooth were within the mean band of the sound teeth as in figure 2e–h. Therefore, in order to avoid making the plots complex, those healthy points are not presented in figure 3. PTR amplitude curves for the fissures in figure 3c showed larger amplitude at all frequencies and a curvature in the mid-frequency range. PTR phases for the carious fissure in figure 3d also showed non-healthy features: a larger phase lag at low frequencies and a steep slope resulting in a crossover with the healthy band at intermediate frequencies. LUM amplitude and phase ($f > 10$ Hz) for the carious spots in figure 3e, f were also higher than the respective healthy bands.

Carious Fissure Revealed Only with PTR and LUM

The mandibular second premolar in figure 4 illustrates the diagnostic ability of PTR and LUM. The tooth had a DIAGNOdent reading of maximum 10 and average visual inspection ranking of 2.2, indicating that a clinician would need to watch or monitor the fissures. There was no indication on the radiographs of any caries being present. Nevertheless, PTR and LUM signals, including all information from the amplitude and phase responses

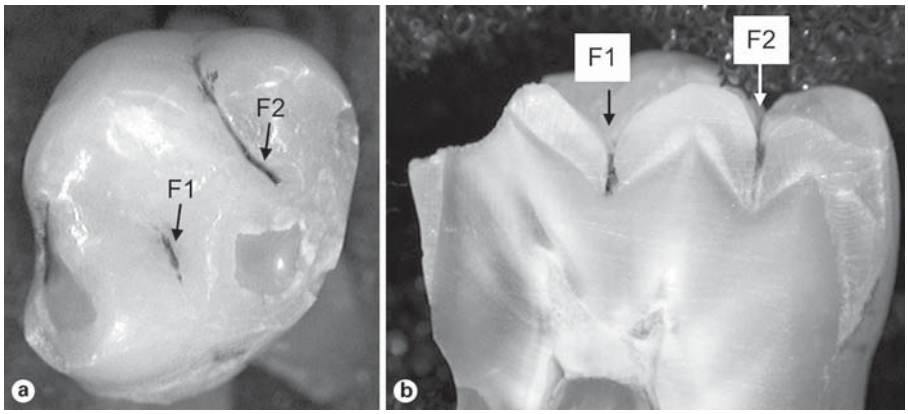

Fig. 3. A carious tooth sample and its PTR and LUM signals using 659 nm excitation: occlusal view of the tooth (**a**); cross-sectioned view of each measurement point, F1 and F2 (**b**); PTR (**c**, **d**) and LUM (**e**, **f**) amplitude and phase frequency scans at all the measurement points with the healthy mean value and population-weighted standard deviation.

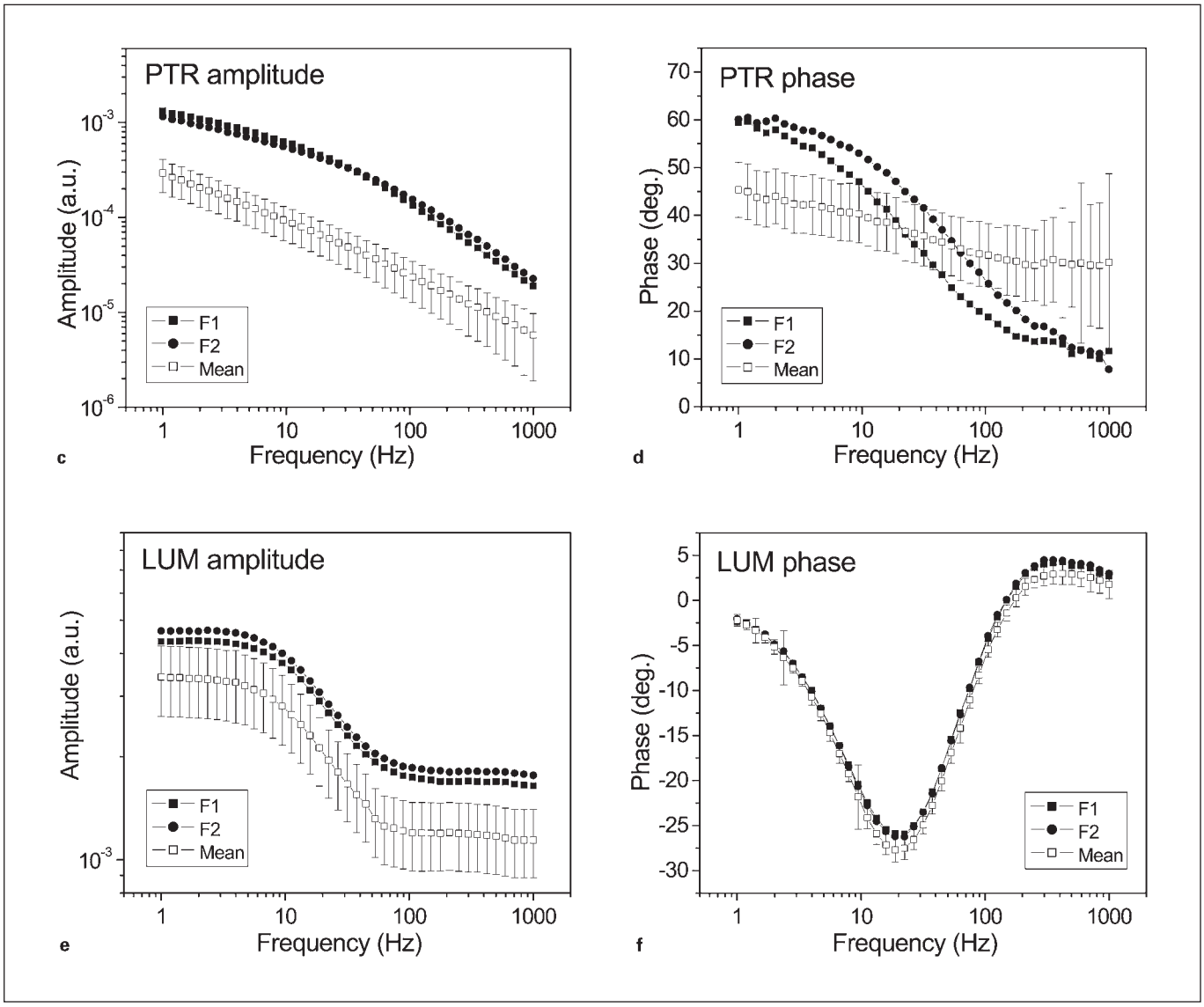

Table 2. Characteristics of frequency scan curves of PTR and LUM

Signal	General characteristics	Converting equation to determine numeric ranking
PTR amplitude	the shape for a healthy spot in log-log plot is almost linear from low frequency (1 Hz) to high frequency (1,000 Hz) unhealthy (demineralized surface, enamel caries or dentin caries) spots show greater amplitude at all frequency ranges compared to healthy spots unhealthy spots show a curvature (greater than healthy spots) in the frequency range of 10–100 Hz in a logarithmic plot	(slope at low frequency) – (slope at high frequency) average of 4 frequencies
PTR phase	the shape for the healthy spot in log (freq.)-linear (phase) plot is almost linear from low frequencies (1 Hz) to high frequencies (1,000 Hz) unhealthy spots show higher phase at low frequency range and the reverse at the high frequency range than healthy spots	[average of phases at 2 low frequencies (1, 6.7 Hz)] – [average of phases at 2 high frequencies (211.4, 1,000 Hz)]
LUM amplitude	both healthy and unhealthy spots show same shape: higher amplitude at low f than at high f unhealthy spots show greater amplitude than healthy ones	average at 3 frequencies (1, 211.4, 501.2 Hz)
LUM phase	high frequency range (> 100 Hz) only, unhealthy spots show larger phase than healthy ones	one phase signal at high frequency (501.2 Hz)

over the entire frequency scan (1 Hz to 1 kHz), indicated that F2 and F3 had caries into dentin. Histological observation results showed that this was, indeed, the case for these two points, as well as for point F1. The signals from fissure F1 showed the influence that fissure geometry, angle of the mouth of the fissure or the direction of the fissure base can have in the generation of PTR and LUM signals. The PTR amplitude of F1 in figure 4f was above the healthy band and the PTR phase in figure 4g also showed clear departure from the healthy band in the high frequency range. This case illustrates the depth profilometric abilities of PTR. Figure 4b shows that the slanted carious fissure F1 was illuminated by the incident laser beam in such a way that the carious region formed a thin surface layer, succeeded by a much thicker healthy substrate enamel layer. In response, the phase of the PTR signal for F1 (fig. 4g) fell within the healthy band at low frequencies as expected from the long thermal diffusion length which mostly probes the healthy enamel sublayer with the carious surface layer as a perturbation to the signal. At high frequencies, however, the (short) thermal diffusion length lay mostly within the carious surface layer and, as a result, the PTR phase emerged below the healthy band above approximately 50 Hz and joined the phases of the carious spots F2 and F3. In principle, the frequency of departure from the healthy band can be used to estimate the thickness of the carious surface layer. PTR and LUM curves of the healthy fissure F4 were located within the healthy band, confirming the histological observations. Again the low curvature PTR phase of F4 lay within the healthy band in a manner similar to the healthy fissures F1–F3 (fig. 2f).

Statistical Analysis: Methodology and Results

In order to assess PTR and LUM as caries diagnostic techniques and compare them (combined and separately) to other conventional probes, sensitivities and specificities were calculated at two different thresholds (D_2) and (D_3) as defined in table 1 for all the diagnostic methods. While the PTR and LUM signals were taken from all 280 occlusal measurement points, only 1 or 2 points on each tooth were assessed by the other examination methods. The visual examination was of the entire occlusal surface and the location of the highest DIAGNOdent reading was recorded, since these formed the diagnostic criteria for the tooth. Therefore, each calculation only used the corresponding measurement points. To create suitable criteria for assessing the carious state via PTR and LUM, the general characteristics of the respective signals and their converting equations, listed in table 2, were used. Those characteristics were established from the experimental results of the frequency scans with carious and healthy tooth samples. In the case of the PTR amplitude, as shown in figure 2e, the shape of the frequency scan

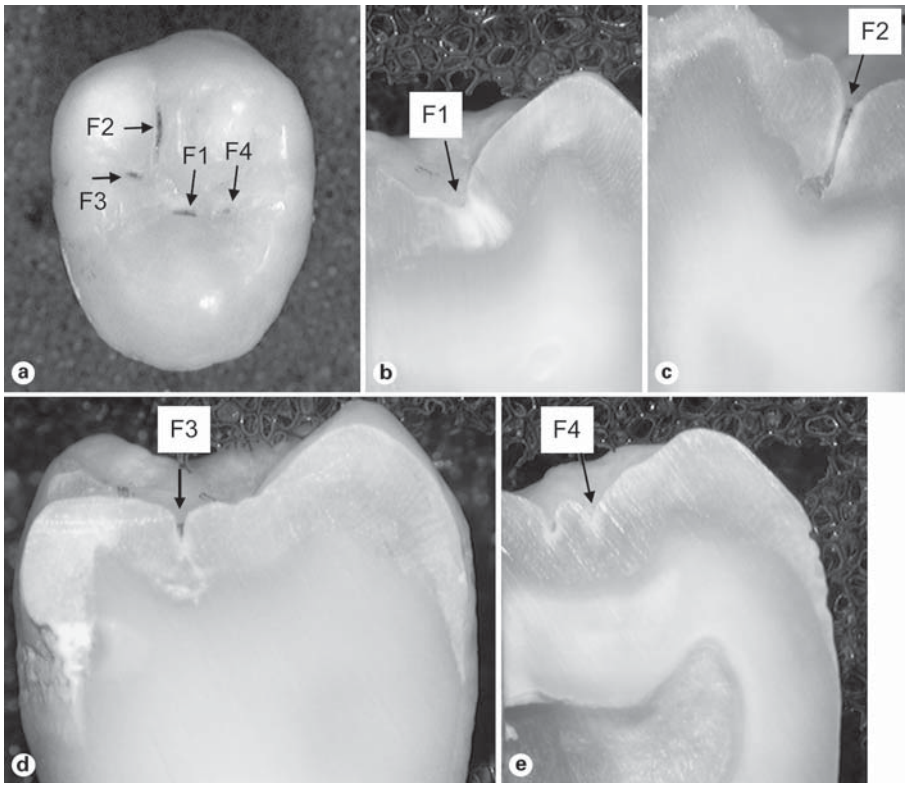

Fig. 4. A carious tooth sample and its PTR and LUM signals using 659 nm excitation. Occlusal view of the tooth (**a**); cross-sectioned view of each measurement point, F1, F2, F3 and F4 (**b–e**); PTR (**f**, **g**), LUM (**h**, **i**) amplitude and phase frequency scans at all the measurement points with the healthy mean value and population-weighted standard deviation.

curve for the healthy spot on a log-log plot was almost linear from low frequency (1 Hz) to high frequency (1,000 Hz) [the absolute value of the slope difference between the high frequency range and the low frequency range on a log-log plot was less than 0.2 log(V)/log(Hz)], while unhealthy spots (demineralized surface, enamel caries or dentin caries) exhibited larger amplitude than healthy spots over the entire frequency range and a pronounced curvature with a 'knee' at certain frequency ranges on the logarithmic plot as shown in figure 3c. The PTR phase shape for the healthy spot on a linear (phase)-log (frequency) plot, as shown in figure 2f, was almost linear across all frequencies (1 Hz to 1 kHz), while unhealthy spots in figure 3d exhibited larger phases at low frequencies and large slopes, crossing the healthy phase range at intermediate frequencies. There was no difference in the LUM amplitude shape between healthy and unhealthy spots, as shown in figures 2g and 3e. The shape of the amplitude curves was consistent throughout, decreasing from low to high frequencies. The LUM amplitude curves for unhealthy spots in figure 3e lie above the healthy band over the entire frequency range. The LUM phase showed slight differences between healthy points (fig. 2h) and carious points (fig. 3f). In general, carious regions exhibited LUM phase lags slightly shifted above the healthy mean throughout the measured frequency range. Healthy spots might exhibit slight deviations, but only at the high frequency end (>100 Hz; fig. 2h, 3f).

We established the mean values for PTR amplitude and phase, and LUM amplitude and phase from all the healthy smooth surface points on the tooth samples. This allowed us to examine the behaviour of healthy tooth structure without the influence of fissure geometry or the effects of varying enamel thickness in the fissure. A series of mean values and standard deviations vs. frequency curves were developed for each signal and plotted for each tooth. This allowed us to compare the behaviour of each probed point to a healthy smooth surface area.

Using these features, characteristic (converting) equations were generated from the plots to yield numeric values defining the state of the teeth as listed in table 2. In addition, out of the entire frequency scan, each signal (amplitude and phase) was examined at 3 frequencies (LUM) or 4 frequencies (PTR) whether it deviated from the healthy norm band, and the number of points that deviated from this band was counted. After calculating

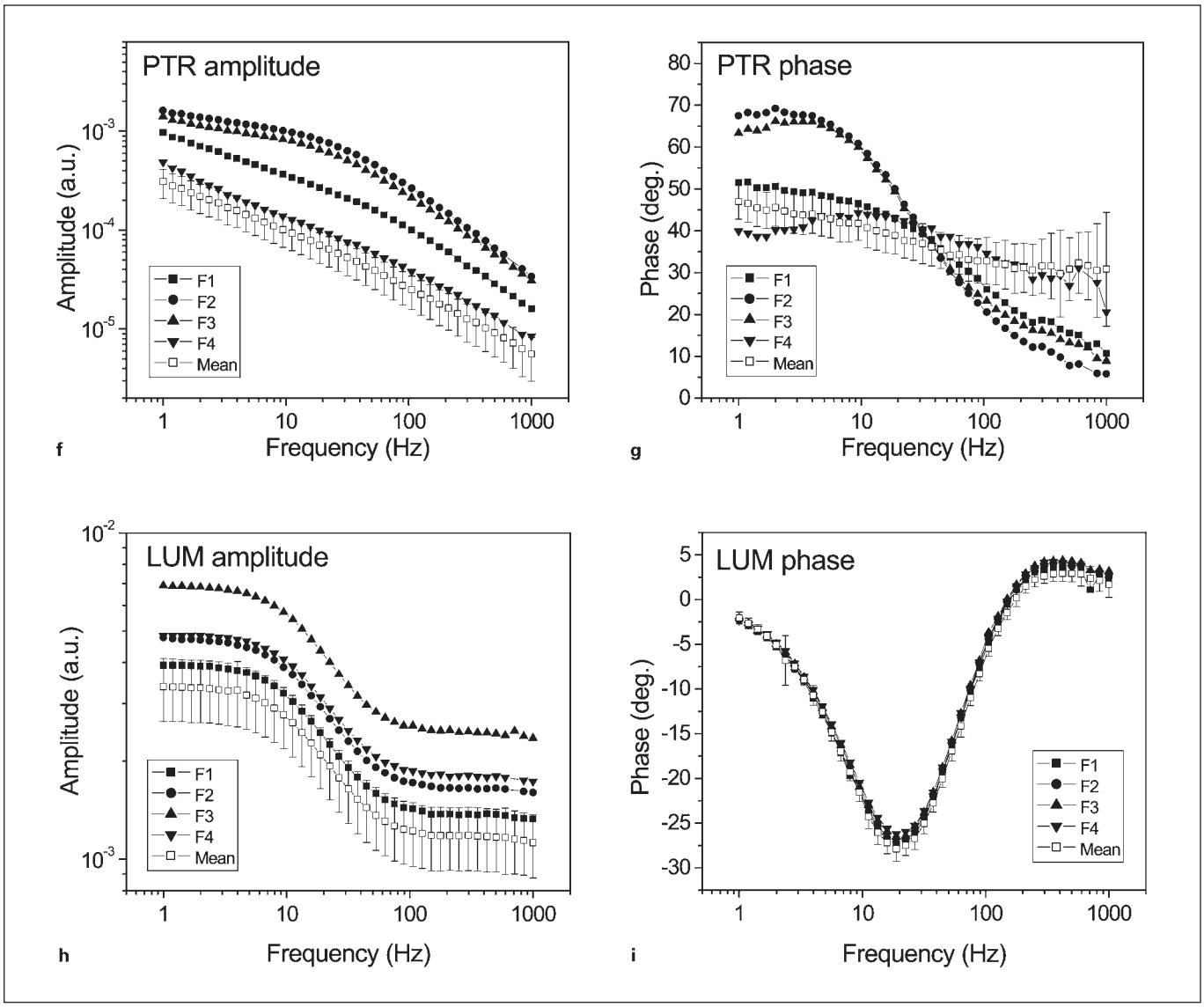

all these values, each number group was normalized so that the assigned numbers in each group had a value between 0 for intact teeth and 1 for the largest carious lesion. Then these normalized numbers were added and used to evaluate the probed spots. Finally, one value per measurement point was recorded, which included all available information of the frequency response. The thresholds of D_2 and D_3 were determined by trial and error to comply with the histological observations as closely as possible.

The results of the statistical analysis are given in table 3. Using the combined criteria of PTR and LUM, the highest sensitivities and specificities, 0.81 and 0.87, respectively, were calculated at the D_2 threshold among all the examination methods. In the cases of PTR-only or LUM-only criteria, sensitivities were between 0.52 and 0.69, while specificities were relatively higher, between 0.72 and 0.86. In agreement with other researchers' findings [Lussi et al., 2001; Alwas-Danowska et al., 2002; Costa et al., 2002; Heinrich-Weltzien et al., 2002], visual inspection resulted in poor sensitivities (0.51 at D_2 and 0.36 at D_3) and particularly high specificities (1.00 at both thresholds). Radiographs also exhibited poor sensitivities (0.29 at D_2 and 0.36 at D_3) and high specificities (1.00 at D_2 and 0.85 at D_3). Additionally, the formalism for obtaining Cohen's kappa for visual inspection was extended

Table 3. Sensitivities and specificities at the caries level of enamel (D_2) and the caries level of dentin (D_3) for various examination methods

Examination method	Sensitivity[a]		Specificity[b]		Size of sample (points, n)
	D_2 threshold	D_3 threshold	D_2 threshold	D_3 threshold	
PTR and LUM combined	0.81 (75/93)	0.79 (26/33)	0.87 (163/187)	0.72 (179/247)	280
PTR only	0.69 (64/93)	0.52 (17/33)	0.86 (161/187)	0.72 (178/247)	280
LUM only	0.60 (56/93)	0.58 (19/33)	0.81 (151/187)	0.77 (189/247)	280
Visual inspection	0.51 (18/35)	0.36 (4/11)	1.00 (17/17)	1.00 (41/41)	52
Radiograph	0.29 (10/35)	0.36 (4/11)	1.00 (17/17)	0.85 (35/41)	52
DIAGNOdent	0.60 (38/63)	0.76 (16/21)	0.78 (53/68)	0.85 (94/110)	131

[a]In parentheses true positive/(true positive + false negative).
[b]In parentheses true negative/(true negative + false positive).

to multiple categories and examiners, as shown in the 'Appendix'. The statistical literature standard (including dental research) is for 2 raters and several categories or for two categories and several raters [Nyvad et al., 1999; Heinrich-Weltzien et al., 2002; Pinelli et al., 2002]. We extended the formalism to an arbitrary number of categories and raters. For the 5 examiners and 10 categories shown in table 1, Cohen's kappa was very low (<0.1), as expected from the higher-than-two input statistical correlations. However, using D_2 or D_3 thresholds, reducing the set of categories to 2, which is similar to the method Nyvad et al. [1999] used, larger kappa values were calculated: 0.30 at D_2 threshold and 0.39 at D_3 threshold. Even these values are too low. Using only results from 2 or 3 examiners among the 5 examiners, Cohen's kappa showed a wide range of values: 0.11–0.48 at D_2 threshold and 0.19–0.71 at D_3 threshold. From these results it can be concluded that Cohen's kappa statistics show poor agreement if there are more than 2 raters, but it can be meaningful when the number of raters remains fixed. The continuous (dc) luminescence method (DIAGNOdent) showed sensitivities of 0.60 at D_2 and 0.76 at D_3; specificities were 0.78 at D_2 and 0.85 at D_3. From table 3 it should be noted, however, that a relatively small subset of all our measurement spots was used for obtaining the visual and radiographic statistics, compared to the much more comprehensive sample sizes used for the other methods, especially for PTR and LUM. In addition, DIAGNOdent measurements were performed with that instrument's fiber-optic waveguide, whereas LUM and PTR measurements used direct incidence of the light on the tooth surface and were subject to variable incidence solid angle limitations.

Wavelength Dependence of Imaging Resolution and Contrast

In order to compare the frequency responses and depth profilometric imaging quality at two different wavelengths, the two lasers (659 and 830 nm) were used with a sample tooth shown in figure 5. Frequency scans were performed at the same spots (P1, P2 and P3) with the two lasers on the visually healthy surface of a mandibular bicuspid (fig. 5a) which, however, hides a large carious cavity on the opposite side, 3–5 mm deep, as revealed in the occlusal and cross-sectional views (fig. 5b, c). The more deeply penetrating 830-nm radiation generated better PTR amplitude resolution and contrast ability (fig. 5d3, d4) than the 659-nm radiation (fig. 5d1, d2) of the irregular white (light scattering) demineralized features surrounding the dark carious pulp tissue at the centre of the scan around the measurement point P2 in figure 5c. The lower PTR amplitude associated with 830 nm excitation was due to the increased optical absorption depth (decreased absorption coefficient with decreasing scattering coefficient) at that wavelength, resulting in decreased optical density (increased illumination volume). In addition to the decreased absorption coefficient, the scattering coefficient decreased as well, leading to increased optical extinction length [Nicolaides et al., 2002]. Among the three probed spots P1–P3, the lower PTR amplitude and smaller phase lag at P3 for both wavelengths (fig. 5e) were probably due to the excessive thinning of the sound dentin and the concomitant loss of source power to the backing (air), which tended to eliminate contributions of infrared emissions from that region, thus decreasing the overall penetration depth contributions to the PTR amplitude and also shifting the thermal-wave centroid clos-

er to the front surface, which resulted in decreasing the PTR phase lag [Jeon et al., 2004]. The LUM scans in figure 5d5, d6 show much reduced resolution and contrast ability to identify subsurface caries.

Overall, the PTR spatial resolution and peak-to-valley contrast of the 830-nm scans for subsurface features several millimetres deep is superior to that for 659-nm scans.

Conclusions

Our data indicate that the PTR amplitude and phase curves exhibit strong curvature when associated with demineralized enamel in fissures. The frequency where the curvature maximum occurs varies from sample to sample. The frequency dependence of the maximum is believed to be a function of the level or condition of the caries and the geometry and depth of the lesion. Unlike LUM, PTR has been proven to have depth profilometric character. With very low modulation frequencies we are able to probe deeper layers (up to 5 mm from the surface) [Jeon et al., 2004]. Table 3 shows that the sensitivity using only PTR or LUM is lower than the specificity. However, combining PTR and LUM, both amplitudes and phases, the sensitivity is much higher than any other methods used in this study.

Using simultaneous non-intrusive, non-contacting frequency-domain PTR and LUM imaging techniques, we have been able to detect carious lesions in the occlusal fissures of posterior human teeth. These investigations have been performed mainly with a near-infrared source (659 nm wavelength) from a semiconductor laser. Additional studies with a longer wavelength were also performed and exhibited enhanced depth resolution. PTR and LUM are able to detect lesions which are neither vis-

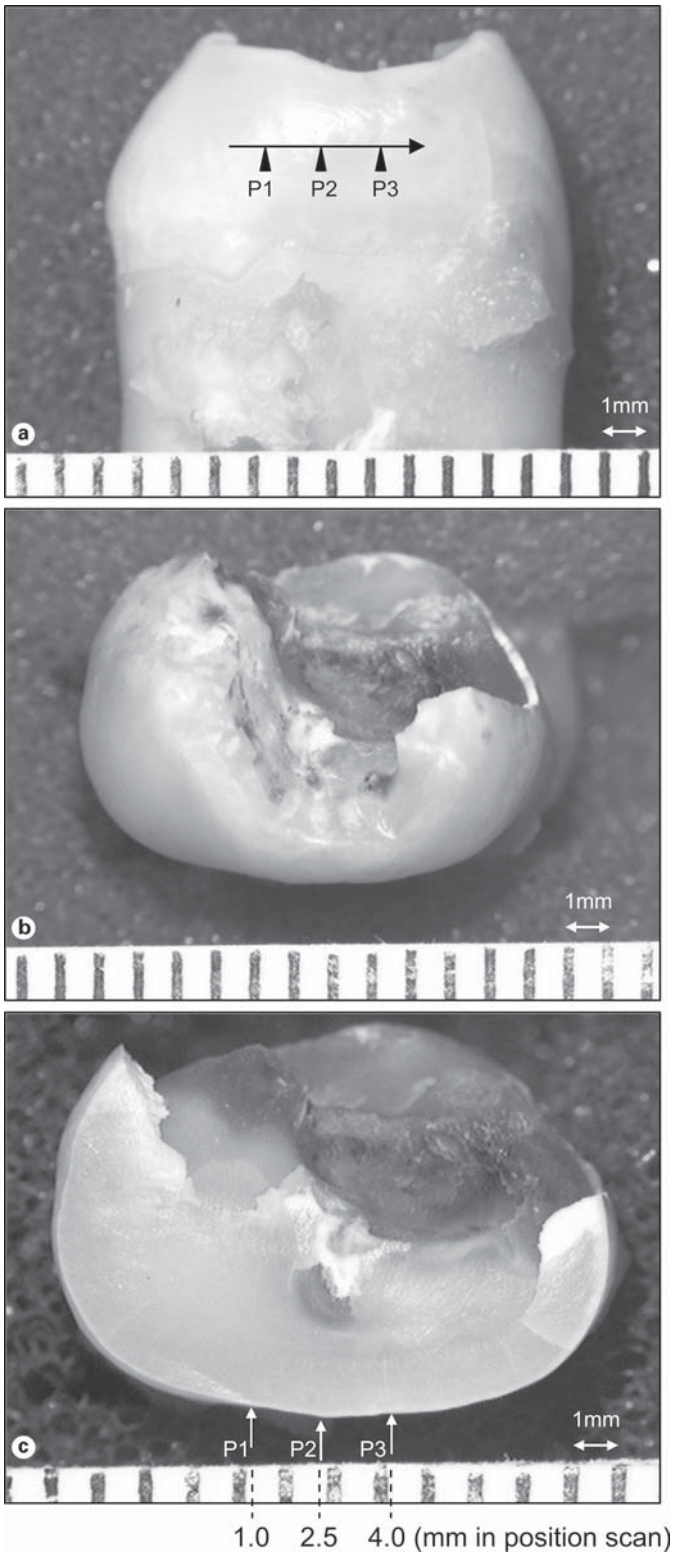

Fig. 5. Photographs, frequency scan and position scan results with 659-nm and 830-nm lasers. **a** Front surface of the tooth with the measurement points indicated (frequency scan: P1, P2 and P3; position scan: horizontal arrow). **b** Top-view of the tooth. **c** Top-view of the cross section at the level of the scan points. **d1**, **d2** PTR position scans, amplitudes and phases with the 659-nm laser. **d3**, **d4** PTR position scans, amplitudes and phases with the 830-nm laser. **d5**, **d6** LUM amplitudes and phases with the 659-nm laser. **e1**, **e2** PTR amplitude and phase frequency scans with the 659-nm laser. **e3**, **e4** PTR amplitude and phase frequency scans with the 830-nm laser.

(For fig. 5d–5e see next pages.)

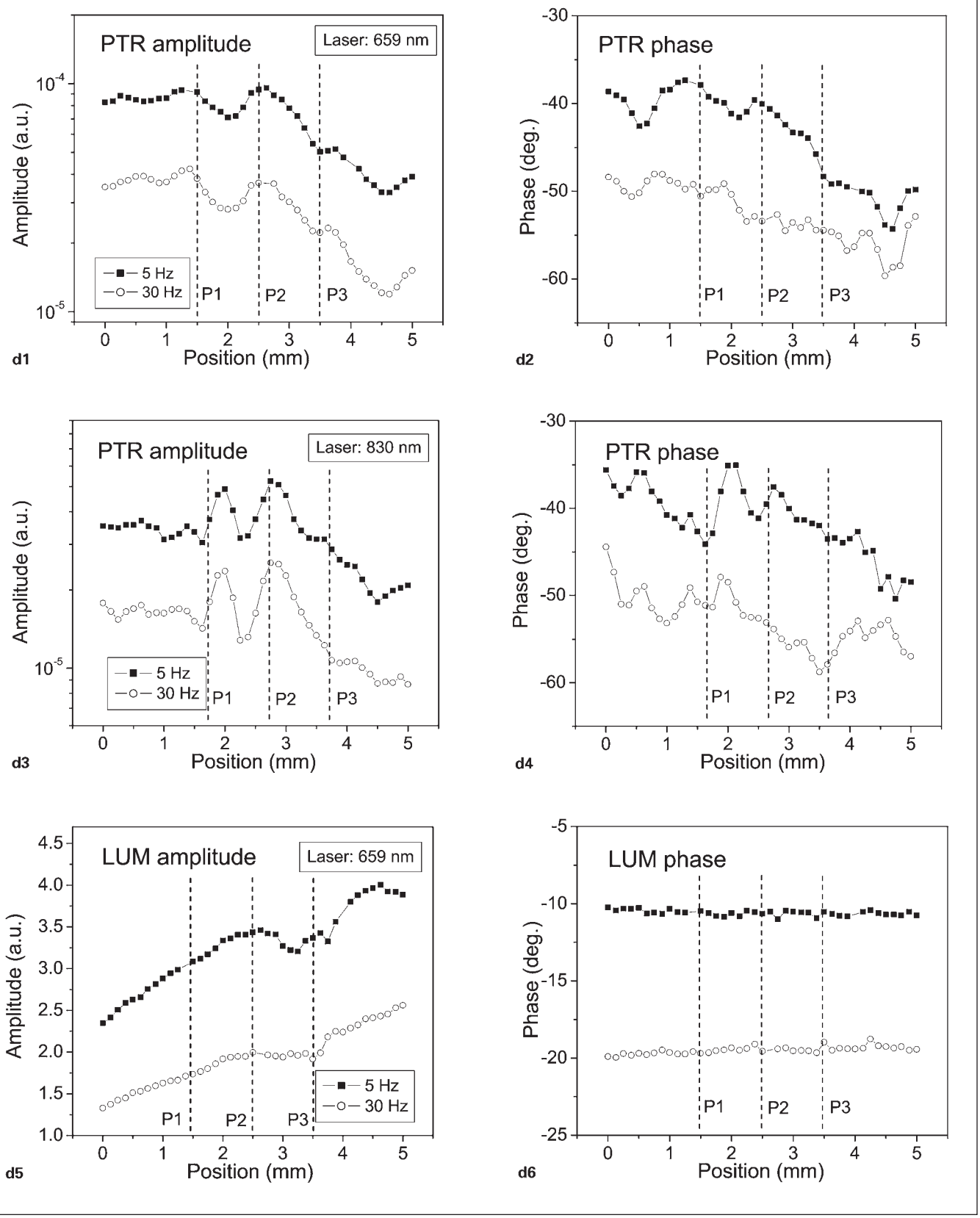
PTR amplitude
Laser: 659 nm
Amplitude (a.u.)
10^-4
10^-5
5 Hz
30 Hz
P1
P2
P3
0 1 2 3 4 5
Position (mm)
d1
PTR phase
Phase (deg.)
-30
-40
-50
-60
P1
P2
P3
0 1 2 3 4 5
Position (mm)
d2
PTR amplitude
Laser: 830 nm
Amplitude (a.u.)
10^-5
5 Hz
30 Hz
P1
P2
P3
0 1 2 3 4 5
Position (mm)
d3
PTR phase
Phase (deg.)
-30
-40
-50
-60
P1
P2
P3
0 1 2 3 4 5
Position (mm)
d4
LUM amplitude
Laser: 659 nm
Amplitude (a.u.)
4.5
4.0
3.5
3.0
2.5
2.0
1.5
1.0
5 Hz
30 Hz
P1
P2
P3
0 1 2 3 4 5
Position (mm)
d5
LUM phase
Phase (deg.)
-5
-10
-15
-20
-25
P1
P2
P3
0 1 2 3 4 5
Position (mm)
d6

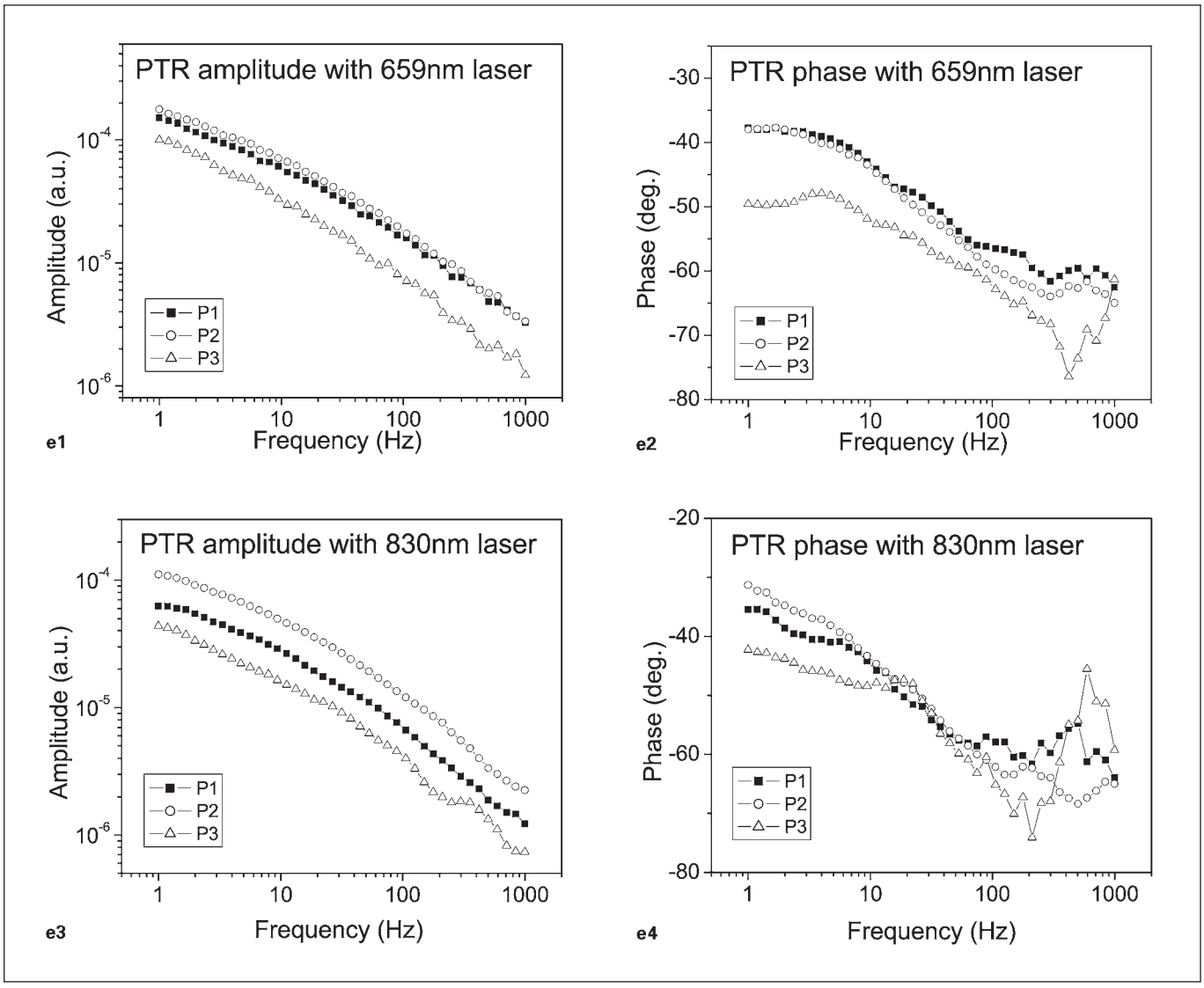

ible, nor detectable with radiographs or with dc luminescence (DIAGNOdent) such as the example of figure 4. PTR's operating physical principle of depth-weighed diffuse photon density waves converted to thermal-wave diffusion, and superposed with direct subsurface radiative infrared (blackbody) emissions generates greater sensitivity and contrast to both the presence of, and changes in, sharp boundaries, a behaviour consistent with thermal-wave diffusive confinement, as well as changes in demineralization of the tooth as compared to the more uniformly depth-integrated LUM. The sensitivity of depth profilometric PTR to the presence of advanced demineralization within an occlusal fissure and the corroboration of the LUM probe, albeit with diminished depth sensitivity, was demonstrated. Thermal-wave confinement within naturally occurring dental layers, such as in the case of variable dentin-enamel junction depth in the proximal surfaces, can be useful in measuring enamel thickness by means of PTR frequency scans at a fixed spot away from high-curvature surfaces. More penetrating laser radiation at 830 nm exhibits better PTR resolution and contrast of scanned subsurface carious features than 659-nm radiation at some expense of signal magnitude and signal-to-noise ratio at high frequencies. The imaging potential of the same features using LUM was shown to be less promising.

In conclusion, the combined wealth of information stemming from four PTR and LUM signals (two amplitudes and two phases), including the availability of detailed frequency-response curve shapes over a wide range of modulation frequencies, was used to examine a large number of spots as a sample of teeth. The combined PTR/LUM approach yielded a statistical sensitivity higher than any of the other methods used in this study, and a specificity comparable to that of dc luminescence diagnostics, although comparisons with DIAGNOdent, radiography and visual inspection results was made using for the latter methods only a subset of the full set of dental spots examined with PTR/LUM. It is concluded that combined PTR and LUM have excellent potential to become a sensitive, non-intrusive dental probe for the diagnosis of near-surface or deep subsurface carious lesions.

Acknowledgement

The support of Materials and Manufacturing Ontario (MMO) with Enabling and Collaborative Contracts is gratefully acknowledged.

Appendix

Cohen's Kappa for Multiple Examiners and Multiple Categories

The accepted formula to calculate Cohen's kappa [Cohen, 1960] is

$$\kappa = \frac{(f_0 - f_c)}{(N - f_c)} \tag{A1}$$

(where f_0 denotes the number of units assessed as belonging to the same category by all the examiners, f_c represents the number of expected frequencies of agreement by chance, and N is the total number of samples assessed. For arbitrary numbers of categories and examiners each parameter can be calculated as follows:

$$f_0 = \sum_{j=1}^{m} f_{0j} \tag{A2}$$

$$f_c = \frac{1}{N^{(n-1)}} \sum_{j=1}^{m} \prod_{i=1}^{n} f_{ij} \tag{A3}$$

where f_{ij} stands for the total number of units the i-th examiner assessed as belonging to category j, regardless of whether it agrees with other examiners' results; f_{0j} denotes the total number of units in j-th category for which all examiners agree; m is the number of categories, and n is the number of examiners.

References

Al-Khateeb S, Exterkate RAM, de Josselin de Jong E, Angmar-Månsson B, ten Cate JM: Light-induced fluorescence studies on dehydration of incipient enamel lesions. Caries Res 2002;36:25–30.

Alwas-Danowska HM, Plasschaert AJM, Suliborski S, Verdonschot EH: Reliability and validity issues of laser fluorescence measurements in occlusal caries diagnosis. J Dent 2002;30:129–134.

Anttonen V, Seppä L, Hausen H: Clinical study of the use of the laser fluorescence device DIAGNOdent for detection of occlusal caries in children. Caries Res 2003;37:17–23.

Brown WS, Dewey WA, Jacobs HR: Thermal properties of teeth. J Dent Res 1970;49:752–754.

Busse G, Walther HG: Photothermal nondestructive evaluation of materials with thermal waves; in Mandelis A (ed): Principles and Perspectives of Photothermal and Photoacoustic Phenomena. Elsevier, New York, 1992, vol 1, pp 205–298.

Clinical Research Associates: Air abrasion caries removal, 5-year status report. CRA Newsl 1999;23:12,2–3.

Cohen J: A coefficient of agreement for nominal scales. Educ Psychol Measurement 1960;20:37–46.

Costa AM, Yamaguchi PM, De Paula LM, Bezerra ACM: In vitro study of laser diode 655 nm diagnosis of occlusal caries. J Dent Child 2002;69:249–253.

Eggertsson H, Analoui M, van der Veen MH, González-Cabezas C, Eckert GJ, Stookey GK: Detection of early interproximal caries in vitro using laser fluorescence, dye-enhanced laser fluorescence and direct visual examination. Caries Res 1999;33:227–233.

Heinrich-Weltzien R, Weerheijm KL, Kühnisch J, Oehme T, Stösser L: Clinical evaluation of visual, radiographic, and laser fluorescence methods for detection of occlusal caries. J Dent Child 2002;69:127–132.

Hibst R, Gall R, Klafke M: Device for the recognition of caries, plaque or bacterial infection on teeth. US Pat 2000;6,024,562.

Hibst R, Konig K: Device for detecting dental caries. US Pat 1994;5,306,144.

Hibst R, Paulus R: Caries detection by red excited fluorescence: Investigations on fluorophores. Caries Res 1999;33:295.

Jeon RJ, Mandelis A, Sanchez V, Abrams SH: Non-intrusive, non-contacting frequency-domain photothermal radiometry and luminescence depth profilometry of carious and artificial sub-surface lesions in human teeth. J Biomed Opt 2004, in press.

Lagerweij MD, van der Veen MH, Ando M, Lukantsova L, Stookey GK: The validity and repeatability of three light-induced fluorescence systems: An in vitro study. Caries Res 1999;33:220–226.

Lussi A, Imwinkelried S, Pitts NB, Longbottom C, Reich E: Performance and reproducibility of a laser fluorescence system for detection of occlusal caries in vitro. Caries Res 1999;33:261–266.

Lussi A, Megert B, Longbottom C, Reigh E, Francescut P: Clinical performance of a laser fluorescence device for detection of occlusal caries lesions. Eur J Oral Sci 2001;109:14–19.

McComb D, Tam LE: Diagnosis of occlusal caries. Part I: Conventional methods. J Can Dent Assoc 2001;67:454–457.

Mandelis A: Diffusion-Wave Fields: Mathematical Methods and Green Functions. Springer, New York, 2001, pp 284–296.

Mandelis A: Review of progress in theoretical, experimental, and computational investigations in turbid tissue phantoms and human teeth using laser infrared photothermal radiometry; in Maldague XP, Rozlosnik AE (eds): Thermosense 24, Proc SPIE, 2002, vol 4710, pp 373–383.

Mandelis A, Munidasa M, Othonos A: Single-ended infrared photothermal radiometric measurement of quantum efficiency and metastable lifetime in solid-state laser materials: The case of ruby (Cr^{3+}:Al_2O_3). IEEE J Quant Electron 1993;29:1498–1504.

Mandelis A, Nicolaides L, Feng C, Abrams SH: Novel dental depth profilometric imaging using simultaneous frequency-domain infrared photothermal radiometry and laser luminescence; in Oraevsky A (ed): Biomedical Optoacoustics. Proc SPIE, 2000, vol 3916, pp 130–137.

Munidasa M, Mandelis A: Photothermal imaging and microscopy; in Mandelis A (ed): Principles and Perspectives of Photothermal and Photoacoustic Phenomena. New York, Elsevier, 1992, vol 1, pp 299–367.

Nicolaides L, Feng C, Mandelis A, Abrams SH: Quantitative dental measurements by use of simultaneous frequency-domain laser infrared photothermal radiometry and luminescence. Appl Opt 2002;41:768–777.

Nicolaides L, Mandelis A, Abrams SH: Novel dental dynamic depth profilometric imaging using simultaneous frequency-domain infrared photothermal radiometry and laser luminescence. J Biomed Opt 2000;5:31–39.

Nyvad B, Machiulskiene V, Baelum V: Reliability of a new caries diagnostic system differentiating between active and inactive caries lesions. Caries Res 1999;33:252–260.

Pinelli C, Serra MC, Loffredo LCM: Validity and reproducibility of a laser fluorescence system for detecting the activity of white-spot lesions on free smooth surfaces in vivo. Caries Res 2002;36:19–24.

Ricketts D, Kidd E, Weerheijm K, de Soet H: Hidden caries: What is it? Does it exist? Does it matter? Int Dent J 1997;47:259–265.

Shi XQ, Tranæus S, Angmar-Månsson B: Comparison of QLF and DIAGNOdent for quantification of smooth surface caries. Caries Res 2001;35:21–26.

Shi XQ, Welander U, Angmar-Månsson B: Occlusal caries detection with KaVo DIAGNOdent and radiography: An in vitro comparison. Caries Res 2000;34:151–158.

Welsh GA, Hall AF, Hannah AJ, Foye RH: Variation in DIAGNOdent measurements of stained artificial caries lesions. Caries Res 2000;34:324.